Advances in Geo-Energy Research

Vol. 14, No. 1, p. 49-63, 2024

Original article

# Rock physical evolution and microscopic flow mechanism of massive energy replenishment in tight oil reservoirs

Zhuoying Dou[1,2], Zhengming Yang[2,3]*, Changchun Dong[4], Haibo Li[2,3], Yimeng Wang[4], Haitao Hou[3]

[1]*University of Chinese Academy of Sciences, Beijing 100049, P. R. China*

[2]*Institute of Porous Flow & Fluid Mechanics, Chinese Academy of Sciences, Langfang 065007, P. R. China*

[3]*Research Institute of Petroleum Exploration & Development, PetroChina, Beijing 100083, P. R. China*

[4]*Jilin Oilfield Research Institute of Petroleum Exploration & Development, PetroChina, Songyuan 138000, P. R. China*

**Keywords:**
Massive energy replenishment
massive water huff and puff
online nuclear magnetic resonance
evolution of physical properties
microscopic flow

**Cited as:**
Dou, Z., Yang, Z., Dong, C., Li, H., Wang, Y., Hou, H. Rock physical evolution and microscopic flow mechanism of massive energy replenishment in tight oil reservoirs. Advances in Geo-Energy Research, 2024, 14(1): 49-63.
https://doi.org/10.46690/ager.2024.10.07

**Abstract:**
Massive energy replenishment presents a practical approach to increase and maintain the formation pressure in tight oil reservoirs. However, the evolution of rock physical properties after this process remains unclear, posing challenges to further elucidate the related microscopic flow mechanism. In the current work, we designed a physical method that uses online nuclear magnetic resonance to simulate the life cycle of "injection, soaking, and production" in massive energy replenishment. The rock physical properties evolution and pore-scale flow mechanism are analyzed by quantitative and visualization methods. Additionally, the influence of injection volume and production pressure difference on oil recovery is clearly defined. The findings suggest that the primary evolution of microscopic pore structure during massive energy replenishment involves microfractures and micropores, promoting the involvement of more pore throats in the flow. However, the flow capacity increase varies at different locations, with a higher increase observed at the inlet than at others. The increase in pseudo-permeability exhibits exponential growth with the injection volume, and its inflection point positively correlates with initial permeability. Massive water huff and puff significantly enhances oil recovery by increasing the pore pressure and flow channels. The apparent energy enhancement and accumulation effect during soaking facilitates oil drained by imbibition to migrate towards the macropores at the outlet in abundance and being enriched. The inflection point of the increase in the recovery degree can be realized by a small pressure difference in production. Importantly, however, considering the carry-over and extrusion effect of injected water on oil droplets, a combination of flooding and soaking is essential to mobilize the fluid in micro-mesopores.

## 1. Introduction

Fluid injection into tight oil reservoirs has been a primary strategy for conventional energy replenishment after years of volume fracturing operations. As a cost-effective medium, water has been extensively employed for this purpose (Sanchez-Rivera et al., 2015). However, achieving the desired effects through conventional fluid injection is challenging due to the rapid depletion of natural energy after fracturing (Todd and Evans, 2016; Milad et al., 2021), as well as the elastic-plastic deformation resulting from continuous changes in the stress field during ongoing production (Thomas and Don, 1972; Vairogs and Vaughan, 1973; David et al., 1994; Wijaya and Sheng, 2020; Radwan et al., 2022). Massive fluid injection has gradually emerged as an effective technique to replenish the formation energy and improve the physical properties of reservoirs in the form of opening microfractures (Bodini et

Yandy Scientific Press

*Corresponding author.
*E-mail address*: dzy935625@163.com (Z. Dou); yangzhm_riped@163.com (Z. Yang); dongcc-jl@petrochina.com.cn (C. Dong); lihaibo05@petrochina.com.cn (H. Li); wangyimeng310@sina.com (Y. Wang); houhaitao69@petrochina.com.cn (H. Hou).

Received July 15, 2024; revised August 12, 2024; accepted September 5, 2024; available online September 10, 2024.

al., 2018; Ji et al., 2023). Because of the qualitative change in the mass transfer rate and quantity between fractures and matrix during massive energy replenishment, understanding the mechanisms behind energy replenishment and subsequent production can provide a fundamental theoretical basis for massive energy replenishment in tight oil reservoirs.

The qualitative relationship found between the injection volume and the recovery degree in water injection development suggests that massive injection increases oil recovery (Zhou et al., 2020; Ma et al., 2022). Taking advantage of the similarity of production characteristics in the mid-to-late stage of volume fracturing and water huff and puff, the enhanced oil recovery technology of massive water huff and puff has been developed. Pilot tests demonstrated that massive water huff and puff can restore the actual formation pressure from 42.29% to 71.40% of the initial formation pressure and increase the maximum daily oil production by nearly tenfold (Qin et al., 2021). Wu et al. (2017) proposed a comprehensive oil recovery mechanism model for massive water huff and puff, which involves the combination of unstable replenishment, soaking for oil production, and unstable displacement. Moreover, they derived the equations for production capacity calculation based on the reservoir engineering method. Li et al. (2022a, 2022c) conducted massive water huff and puff physical simulation experiments on full-diameter cores. They concluded that the recoverable fluid in massive water huff and puff tended to exhibit Darcy flow, leading to a linear decrease in recovery degree with each cycle and a gradually declining recovery efficiency. However, the overall recovery demonstrated significantly superior performance compared to moderate water huff and puff. These works only focused on the oil recovery mechanism and the effect of massive water huff and puff from a qualitative perspective, thus they could not characterize the microscopic flow details within the cores. This necessitates more research on the energy replenishment mechanisms and microscopic analysis.

Furthermore, fluid injection on a large scale or at high pressure can reduce the effective stress in reservoirs. The opening of microfractures leads to nonlinear changes in the elastic modulus of rocks and has a significant impact on the stress-dependent pore elastic response (Pearse et al., 2014; Norris et al., 2015). Consequently, it is crucial to investigate the evolution of rock physical properties (e.g., microscopic pore structure and permeability) following massive energy replenishment, in order to attain a more comprehensive understanding of fluid flow mechanisms during production. Since Hagoort (1981) first proposed the concept of water-induced fractures, extensive studies have been conducted on the water-induced fractures of long-term water injection in conventional reservoirs, primarily by means of numerical simulations and analytical methods. These studies encompass the fracture propagation mechanism (Abou-Sayed et al., 2005), the relationship between fracture state and tip strength factor (Van Den Hoek et al., 2008), and the impact of fracture orientation on oil recovery (Gadde and Sharma, 2001). In recent years, the issue of water-induced fractures has gradually extended from conventional reservoirs to unconventional reservoirs along with the shift in development objectives. Based on information such as well-water breakthrough and tracer monitoring with obvious directionality and the interpretation of curve characteristics in injection well testing, Wang et al. (2015b) proposed that dynamic fractures are geological attributes of long-term water injection development in ultra-low permeability oil reservoirs. Nevertheless, it is essential to recognize that the influence of massive water injection on the stress field differs from long-term water injection, and that there is a difference between conventional and unconventional reservoir development methods. After large-scale volume fracturing operations in tight reservoirs, increasing the injection pressure to augment the injection volume can effectively stimulate and activate pre-existing closed microfractures rather than generate new fractures (Van Den Hoek, 2002; Wang et al., 2018a, 2018b). It can be concluded that when the injection pressure exceeds the actual horizontal principal stress in the connection direction of a specific injection-production well, microfractures will be opened in the connection direction. Therefore, reaching the breakdown pressure of rocks is unnecessary (Wang et al., 2015a). Obviously, reassessment and repositioning for the effects of massive energy replenishment on rocks is imperative.

This paper establishes a novel physical simulation as an experimental method for integrating "injection, soaking, and production" to simulate dynamic flow in massive energy replenishment based on online nuclear magnetic resonance (NMR). The relationship between injection volume and pressure is given and the evolution of full-scale pore space and permeability is revealed. Afterwards, the fluid movability and flow mechanism of massive water huff and puff are analyzed using quantitative and visualization methods according to NMR $T_2$ and layered $T_2$ spectra. Moreover, the effects of injection method, injection volume, and production pressure difference are investigated on the reservoir development effect.

## 2. Materials and methods

Massive energy replenishment can be subdivided into two stages: Pressurized energy replenishment and depressurized production. Therefore, the experiments of this paper were designed in two parts: Regarding the evolution of physical properties and massive water huff and puff.

### 2.1 Samples

Cylindrical cores were drilled from the same layer and block of Jilin Oilfield in the Songliao Basin, which exhibited similar physical properties. The target formation is the Fuyu formation belonging to the fourth member of Lower Cretaceous Quantou, a large-scale river deltaic depositional system (Sun et al., 2012, 2015). It mainly consists the I and III sand groups, with monolayer thicknesses ranging between 2∼4 m and 4∼10 m, respectively. The reservoir as a whole is a typical tight sandstone reservoir, and the rock is mainly feldspathic clastic sandstone with low quartz content. The average wetting angle distribution indicates its preferential hydrophilicity. Table 1 displays the physical properties of samples. Parallel samples (P1 and P3) were taken for the pilot tests on massive energy replenishment and as a reference for

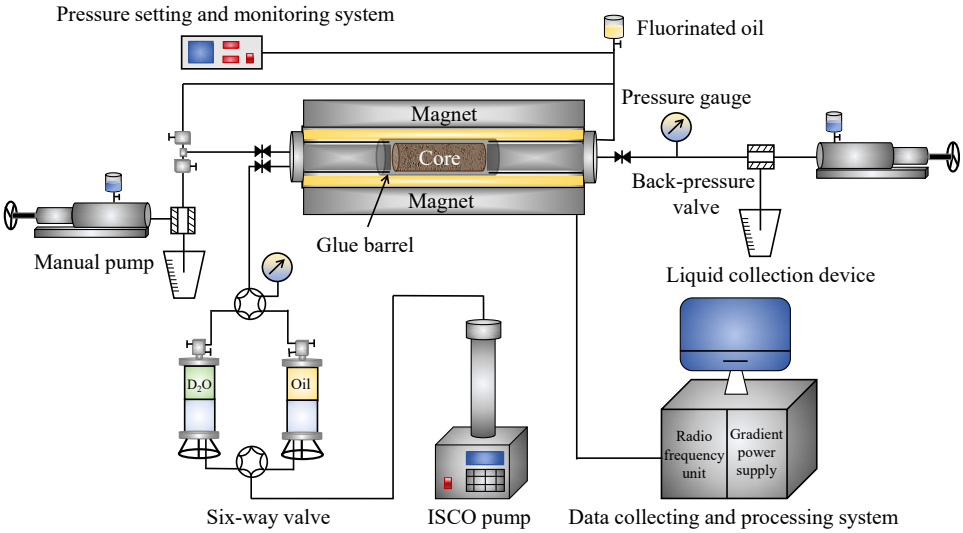


**Fig. 1**. Diagram of the online NMR physical simulation of massive energy replenishment.

**Table 1**. Physical properties of samples.

| No. | Length (cm) | Diameter (cm) | Porosity (%) | Permeability ($10^{-3}$ μm$^2$) |
|---|---|---|---|---|
| Q1 | 7.04 | 2.50 | 11.97 | 0.064 |
| Q2 | 4.89 | 2.53 | 9.92 | 0.085 |
| Q3 | 6.92 | 2.50 | 8.52 | 0.106 |
| Q4 | 7.20 | 2.50 | 12.07 | 0.097 |
| P1 | 6.94 | 2.50 | 8.39 | 0.064 |
| P3 | 7.31 | 2.51 | 7.20 | 0.106 |

the high accuracy and reliability of the experimental results.

## 2.2 Fluid system

The experimental gases for porosity and permeability testing included helium and nitrogen with a purity of 99.9%. The experimental oils were simulated oil and fluorinated oil. Simulated oil is an experimental medium, whose physical properties are consistent with those of crude oil under field conditions, presenting a viscosity of 2.5 mPa·s and a density of 0.9 g/cm$^3$ at 25 °C. Fluorinated oil is an externally circulating medium that provides confining pressure for the online NMR system and does not generate any NMR signal. Due to the significant difference in physical properties between fluorinated oil and simulated oil, the experimental water was deuterium water ($D_2O$) without NMR signals. It has a purity of 99.9% and a mineralization of 30,000 mg/L. Therefore, the detected NMR signal can be solely attributed to the simulated oil.

## 2.3 Experimental setup

The experimental setup mainly included a high-temperature and high-pressure online NMR test system, a pressure setting and monitoring system, and a fluid displacement system (Fig. 1). Among them, the online NMR test system is the primary place for the massive energy replenishment experiment, enabling real-time dynamic monitoring during the whole process of fluid migration via a data acquisition system. It reduces the uncertainties affecting experimental accuracy caused by stress release and changes in oil saturation due to the frequent core removal in conventional physical simulation methods. The pressure setting and monitoring system provides confining pressure by fluorinated oil circulation. The fluid displacement system primarily comprises a piston container, ISCO constant speed and pressure displacement pump, manual pump, and pressure gauge, among other devices.

## 2.4 Testing design

Tight oil cores exhibit significant capillary pressure and limited water injection capacity, necessitating the consideration of injection pressure as an indicator for evaluating the injection capacity (Cheng et al., 2020). Besides, previous studies have demonstrated that larger water injection volumes lead to higher injection and formation pressures (Zhao et al., 2015). Therefore, this study considers injection pressure to represent variations in injection volume, with five points designed based on actual formation pressures and different pressure maintenance levels within the Jilin Oilfield, namely, 16 MPa (current formation pressure, 70% of pressure maintenance), 19 MPa (90% of pressure maintenance), 22 MPa (initial formation pressure), 25 MPa (overpressure), and 27 MPa (overpressure). Furthermore, given that simulated oil is the sole fluid containing NMR signal within cores, it is employed instead of water to conduct experiments on the evolution of physical properties and to investigate the energy replenishment mechanism.

Samples with varying permeability (Q1∼Q3) were selected to establish an estimation criterion for injection volume and pressure (Fig. 2). Injection volume was determined by the volume difference in the displacement pump between pressurized and injection stability, which was then normalized according to the pore volume. In the Jilin Oilfield, the injection volume

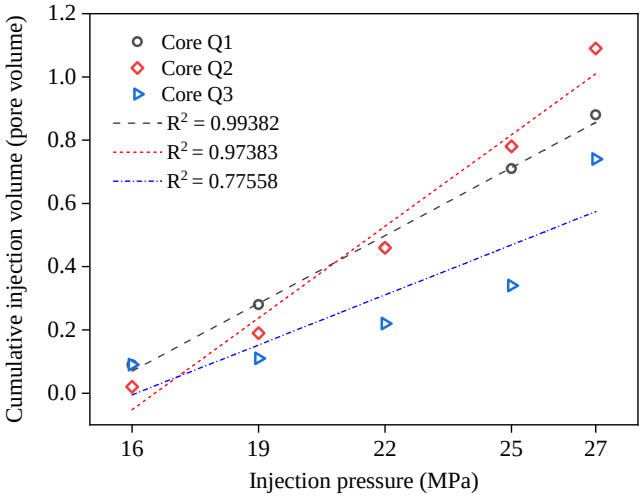


**Fig. 2**. Estimation criterion for the injection volume and injection pressure.

had been estimated based on the pore volume of a single-well-controlled reservoir with a permeability of $0.85 \times 10^{-3}$ μm$^2$. Significantly higher results were obtained compared to the actual injection volume, meeting the requirement for massive injection. Simultaneously, the pilot tests demonstrated the opening of microfractures. Therefore, the injection pressure design method employed in this study is a feasible strategy to reflect massive injection at the centimeter level of cores. It addresses the limitations of indoor physical simulation in designing the injection pressure alone, but it cannot be combined with the injection volume estimation in the field (Li et al., 2022c).

## 2.5 Experimental procedure

### 2.5.1 Evolution of physical properties

Samples Q1∼Q3 were used to conduct experiments on the evolution of physical properties using simulated oil as the injection medium. The specific experimental steps were as follows:

1) Sample preparation: The sample was dried after oil and salt washing, followed by the testing of fundamental physical properties. Additionally, basal NMR testing was performed.
2) $D_2O$ saturation: The sample was subjected to vacuuming for a minimum duration of 6 h, followed by vacuum saturation with $D_2O$ for 1 h. Subsequently, the sample was transferred to a piston container filled with $D_2O$ and pressurized at 16 MPa for 24 h to replicate the formation conditions. At late saturation, weight tests with three replicates were conducted at 16, 20 and 24 h. Saturation was considered to be completed when the variation in weight was negligible. NMR data was acquired upon saturation completion.
3) Simulated oil saturation: The sample was saturated with simulated oil in the core holder until no water was produced at the outlet and a stable weight was achieved, followed by aging treatment for 3 d. Then, NMR data were examined to assess saturation.
4) Preparation: The saturated sample was loaded into online NMR equipment, a confining pressure of 29 MPa was applied, and the back and inlet pressures were increased to 12 MPa for initial NMR data testing.
5) Massive liquid injection: A constant back pressure of 12 MPa was maintained while increasing the inlet pressure to 16 MPa as a first test point due to the effective fluid migration and displacement within the core under a pressure difference of 4 MPa. This ensured the accurate capture of changes in the NMR signal. NMR data were collected during the injection process until the flow rate of the displacement pump stabilized. The final-state NMR data were obtained under the actual injection pressure. The inlet pressure was sequentially increased to 19, 22, 25 and 27 MPa while maintaining a displacement pressure difference of 4 MPa and simultaneously increasing the back pressure until all designated points had been tested.
6) The samples were replaced and the procedures 1)∼5) were repeated.

### 2.5.2 Massive water huff and puff

In order to further investigate the impact of physical properties evolution on the recovery mechanism and effect after massive energy replenishment, this study innovatively took the back pressure at the inlet to replace the medium under pressure maintenance conditions based on the aforementioned experimental system. Q1 was taken to conduct a massive water huff and puff experiment to analyze dynamic development characteristics in different production stages. Simultaneously, Q4 from the same well was taken as a control group for moderate water huff and puff.

The injection pressure of massive water huff and puff was 27 MPa. The specific experimental procedures were as follows:

1) Medium replacement: After the experiment on the evolution of physical properties taking Q1, the outlet back pressure was set to 27 MPa and the inlet back pressure was adjusted to 26 MPa by a manual pump. The valve for the simulated oil was closed, while the valve for $D_2O$ was opened. Subsequently, the displacement pump was switched to a constant-speed mode with a rate of 10 mL/min to replace $D_2O$ rapidly. The process was continued until the collected liquid became clear, indicating the completion of medium replacement.
2) Soaking simulation: The displacement pump was set to a constant pressure of 27 MPa and the manual pump at the inlet was closed for soaking, followed by NMR testing.
3) Production simulation: After 2 h of soaking, NMR data were collected. The production pressure difference was maintained at 4 MPa by reducing the back pressure to 23 MPa. NMR data were continuously monitored until changes in the spectra were negligible, indicating the completion of production under the actual production pressure difference. Subsequently, the back pressure was sequentially reduced to 19 and 12 MPa, resulting in production pressure differences of 8 and 15 MPa, respectively.

The injection pressure of moderate water huff and puff

was 16 MPa, indicating the maintenance of actual formation pressure. The sample preparation followed a similar procedure as Steps 1∼3 in the experiments on the evolution of physical properties and will not be reiterated here. The experimental procedures were as follows:

1) Preparation: The saturated Q4 was loaded into the setup with a confining pressure of 19 MPa, accompanied by inlet and back pressures of 12 MPa. Subsequently, the initial state NMR data were acquired.
2) Soaking simulation: The inlet and back pressures were simultaneously increased to 16 MPa for soaking and the acquisition of NMR data.
3) Production simulation: After 2 h of soaking, NMR data were obtained. The production stage followed a similar procedure as in massive water huff and puff (Procedure 3)). The back pressure was reduced by maintaining the production pressure difference at 4, 8 and 15 MPa, while the corresponding NMR data were collected.

## 2.6 Result tracking

Variations in the NMR $T_2$ spectra among different states effectively indicate changes in oil saturation within the core according to the testing principle. Accordingly, a result tracking method was established for massive energy replenishment.

The relative increase in oil saturation characterizing the evolution of pore structure during massive fluid injection is expressed as:

$$C_{ij} = \frac{A_{ij} - A_{oj}}{A_o} \times 100\% \quad (1)$$

where $i$ represents the different injection pressures; $j$ represents the different-sized pores; $C_{ij}$ represents the relative increase in oil saturation, %; $A_{ij}$ represents the signal of different-sized pores under different injection pressures; $A_{oj}$ represents the signal of different-sized pores in the initial state; and $A_o$ represents the total signal in the saturated oil state.

Due to the coexistence of Darcy and non-Darcy flow in rocks following massive fluid injection, the accurate tracking of absolute permeability becomes challenging. Therefore, pseudo-permeability is employed to approximate the evolution of flow capacity (Chevalier, 2013):

$$K = \frac{\mu L Q}{A \Delta p} \times 10^2 \quad (2)$$

where $K$ represents the pseudo-permeability, $10^{-3}$ μm$^2$; $\mu$ represents the fluid viscosity, mPa·s; $L$ represents the length of sample, cm; $Q$ represents the fluid volume passing through sample per unit time, cm$^3$/s; $\Delta p$ represents the pressure difference between the ends of sample, MPa; and $A$ represents the cross-sectional area of sample, cm$^2$.

The recovery degree of different-sized pores in different production stages is:

$$E_{kj} = \frac{A_{kj} - A_{oj}}{A_o} \times 100\% \quad (3)$$

where $k$ represents the different production stages; $E_{kj}$ represents the recovery degree, %; and $A_{kj}$ represents the signal of different-sized pores in different production stages.

# 3. Results and discussion

The positive correlation between NMR transverse relaxation time ($T_2$) and pore size has been mathematically proven in rocks. Based on the characteristics of NMR $T_2$ spectra distribution in our experiments and previous research(Golsanami et al., 2016; Umeobi et al., 2021), the pores are classified into three categories: micro-, meso- and macropores, corresponding to $0.01 \leq T_1 < 1$ ms, $1 \leq T_2 < 100$ ms, and $T_2 \geq 100$ ms, respectively.

## 3.1 Physical properties response

### 3.1.1 Pore structure

Given the completion of saturation in all samples, the variations in oil saturation combined with pore pressure during massive energy replenishment can indicate the evolution of pore structure. Figs. 3 and 4 illustrate the response of pore structure to injection volume.

These results show different influences of the injection volume on different-sized pores. With dynamic changes in the injection pressure, the left and right peaks of NMR $T_2$ spectra change significantly, while the middle exhibits continuous fluctuations. This observation suggests that the injection volume primarily affects micropores and macropores, while it has a negligible impact on mesopores. The shaded region in the right peak gradually expands towards the upper right as the injection pressure increases, and even a new peak emerges (Figs. 3(b) and 3(c)), demonstrating the transition from the absence to the presence of oil signal. The relative increase in macropores for the three cores were 13.50%, 25.41% and 19.89%, respectively (Fig. 4). It is noteworthy that, in a low permeability oilfield located in Songliao Basin, the critical pressure required to open the closed microfractures along the maximum horizontal principal stress direction was determined as 19.4 MPa (Wang et al., 2015a). Combined with saturation completion in the experimental procedure, given the same sample source and peak location, this observation concludes that microfractures can be opened during massive energy replenishment, and the extent of microfracture opening is positively correlated with injection volume. However, the right peaks in Q1 and Q3 spectra nearly coincide at the injection pressures of 25 and 27 MPa (Figs. 3(a) and 3(c)), which indicates that microfracture opening has reached its upper limit.

It can be observed that microfracture opening in cores with lower permeability gradually increases with the injection volume rising (Fig. 4(a)). In contrast, cores with higher permeability exhibit a high level of rapid opening during the initial injection, followed by a steady rise (Figs. 4(b) and 4(c)). This is primarily attributed to pore structure evolution and mechanical processes. The study block is preferentially hydrophilic with a critical radius. Pores with a radius smaller than this are predominantly occupied by water, while larger pores contain a bound water film (Anderson, 1987). Lower permeability leads to a higher relative proportion of water-filled pores and a more significant influence of the effective pore throat radius on flow resistance due to the smaller overall pore size distribution. Additionally, poor connectivity between

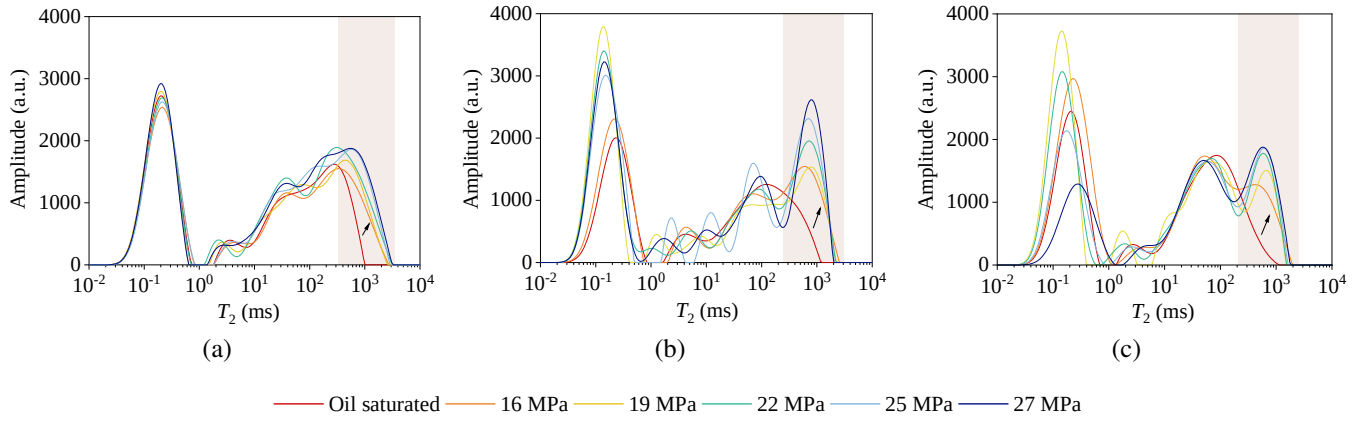


**Fig. 3**. NMR $T_2$ spectra for core samples: (a) Q1, (b) Q2 and (c) Q3.

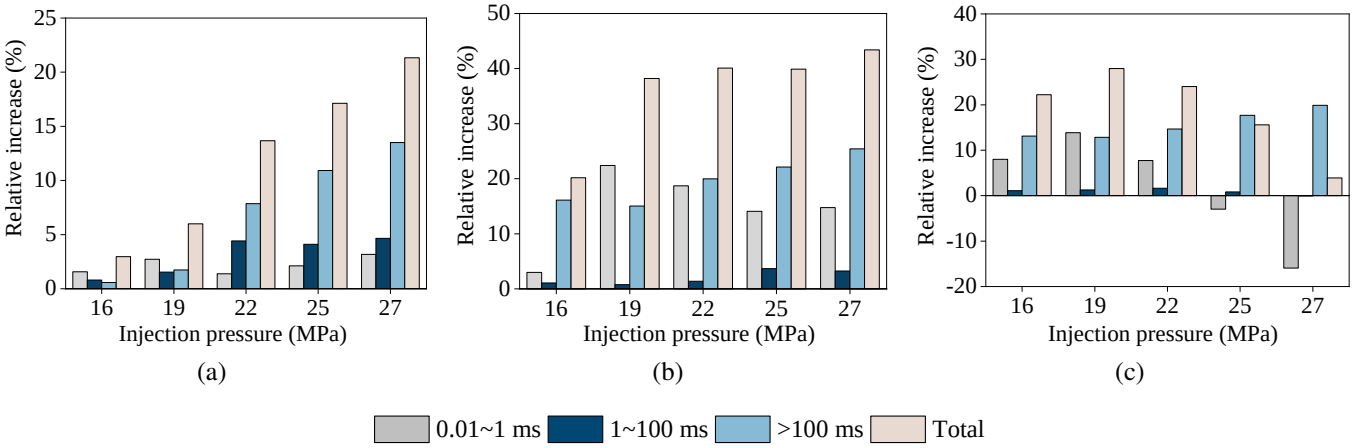


**Fig. 4**. Quantitative analysis of pore structure evolution: (a) Q1, (b) Q2 and (c) Q3.

pores and throats increases the likelihood of stuck fluid and restricts fluid sweep to smaller pores. As a result, fluid enriches primarily in relatively larger pores for a continuous increase in pore pressure with a lower deformation of macropores, the opening of microfractures, slight increments in oil saturation within mesopores, and negligible change in micropores (Figs. 3(a) and 4(a)). Due to the limited number of closed microfractures and the mechanical properties, an upper limit exists for pore pressure increase and the opening of microfractures concerning the injection volume.

It can be found that higher permeability leads to stronger connectivity, broader pore size distribution and the diminished influence of bound water film. Therefore, with increasing injection volume, the injected fluid can increase the sweep ability towards matrix pores. Consequently, larger pores experience deformation due to the stress effect from the slow pore pressure rise. This phenomenon is manifested as an increase in fluid saturation within micropores, as shown in Figs. 4(b) and 4(c). Part of the increasing injection volume enhances the elastic energy of deformed pores. Therefore, a larger injection volume is required to elevate the pore pressure to sustain the microfracture opening (Fig. 3(b)). The deformation of pores controlled by a small throat is greater than that of a large throat, and pores with larger deformation are more challenging to recover due to the same elastic limit. Combined with the rock properties and feldspar dissolution pores (Zhong et al., 2020), certain pores are difficult to recover, causing weakened flow capacity. Consequently, Q2 exhibits stronger deformation than Q3, and Q3 facilitates flow in micro-mesopores with a negative oil saturation (Figs. 3(c) and 4(c)). However, the re-entry of injected fluid into these pores becomes difficult after initial flow due to wettability and capillary forces. This leads to a gradually developing mass balance via the formation of a preferential channel between microfractures and matrix pores and the appearance of a challenging pressure elevation in larger pores. Thus, microfracture opening reaches its upper limit.

During massive energy replenishment, microfracture opening dominates the evolution of pore structure, and its upper limit corresponds to an optimal fluid injection volume. Based on rock debris, Li et al. (2022c) inferred that microfractures are induced by high-pressure water injection. However, our findings offer a factual foundation supported by quantitative analysis for the opening of microfractures. Mesopores are essential channels for fluid migration between micropores and macropores, maintaining a dynamic balance of fluid volume

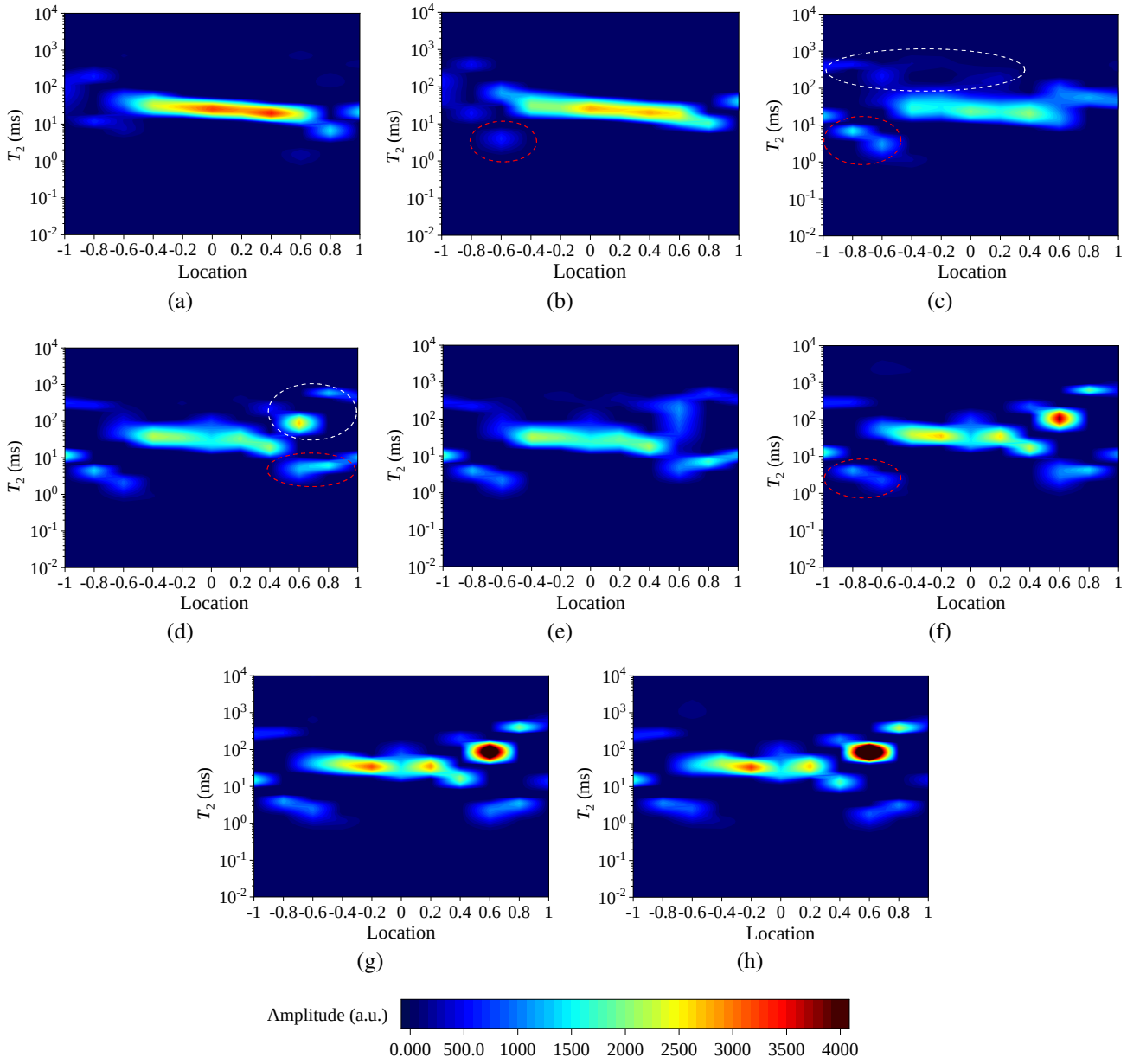


**Fig. 5**. Fluid migration of Q2 during massive injection: (a) Initial state, (b) 16 MPa (1 h), (c) 16 MPa (2.5 h), (d) 19 MPa (1.5 h), (e) 19 MPa (2.5 h), (f) 22 MPa (2 h), (g) 25 MPa (2 h) and (h) 27 MPa (2 h).

and pressure as long as the flow state is maintained. Increased fluid injection volume yields three manifestations of micropores: no significant change, increased quantity, and enhanced flow capacity, with the likelihood of occurrence increasing with growing permeability.

### *3.1.2 Fluid migration*

The impulse sequence of NMR layered $T_2$ is highly sensitive to the mobile fluids in porous media. Layered $T_2$ spectra can track the dynamic change in oil content in varying pores and cross-sections to achieve the visualization of fluid migration. Fig. 5 illustrates the layered $T_2$ spectra of Q2 with increasing injection volume. Fluid injection occurs from right to left, and a total of 11 layers represent corresponding cross-sections ranging from $1 \sim -1$.

Massive energy replenishment can be divided into two stages. Stage I involves an injection pressure range of $16 \sim 19$ MPa, characterized by the initial opening of microfractures and the deformation of certain macropores due to a small injection volume. At this stage, the low pore pressure induces compression or the closure of certain macropores and microfractures with the original oil distribution under intense stress conditions (red circle, Fig. 5(b)). Additionally, lower permeability leads to a slow pressure propagation rate, resulting in more intense stress at the outlet than the center and inlet, noticeably weakening the flow capacity. As the injection time and volume increase, a pressure-out area forms at the inlet while microfractures begin to open initially. Consequently,

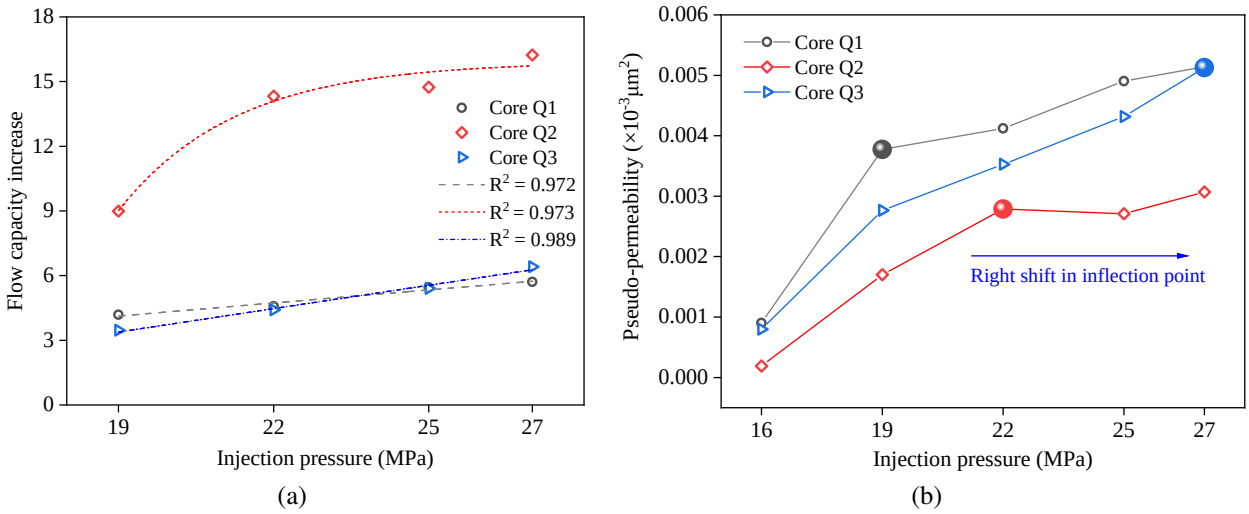


**Fig. 6**. Evolution of permeability: (a) Fitted curve of the increase in flow capacity under varying injection pressures and (b) pseudo-permeability at each injection pressure.

both the flow channel and the fluid-solid contact area expand, leading to a larger pressure sweep area (white circle, Figs. 5(c) and 5(d)). Moreover, a gradual involvement of matrix micropores in the flow is observed (red circle, Fig. 5(d)). Stage II corresponds to an injection pressure range of 22 ~ 27 MPa, characterized by rapid strengthening in the opening of microfractures and elastic recovery on deformation due to the massive fluid injection. Upon increasing the injection volume, microfractures continue opening at the inlet, facilitating the inflow of injected fluid into matrix pores under various forces, such as inertial force, viscous force, and the fracture-matrix pressure difference. Thus, fluid distribution within the pores changes continuously. As pore pressures rise during this stage, there is a gradual recovery in elastic deformation (red circle, Fig. 5(f)). Although oil content decreases over time within these specific-sized pores, it does not entirely disappear, indicating that the flow capacity cannot be restored to its initial state.

Massive energy replenishment can increase the involvement of more pore throats in the flow, with varying increases in flow capacity at different locations. Notably, the inlet exhibits a higher capacity for flow increase than others, while the outlet may experience potentially irreversible deformation. Therefore, it is crucial to regulate production pressure differences in practice to prevent the significant stress sensitivity within the near-well zone of production wells under intense stress, which could reduce the flow capacity.

### *3.1.3 Permeability*

Permeability is a critical parameter that characterizes the fluid flow capacity in porous media and influences the energy replenishment effect. Pseudo-permeability was evaluated according to Eq. (2) to track the flow capacity at different injection volumes (Fig. 6). The increase in flow capacity was subsequently obtained by normalizing the pseudo-permeability to its value at 16 MPa. Fig. 6(a) presents the fitted curve of the increase in flow capacity under varying injection pressures, which reveals an exponential trend. The above discussion emphasizes that massive energy replenishment can open closed microfractures. The flow capacity under massive liquid injection was observed to be 5.71-16.23 times to its response under intense stress. Permeability is highly sensitive to the pore size (Haghi et al., 2018). Therefore, the flow capacity of cores with greater deformation exhibits a more significant increase (Q2) after elastic recovery.

Pseudo-permeability and initial permeability have a specific correlation during massive energy replenishment (Fig. 6(b)). A higher initial permeability leads to a delayed inflection point of pseudo-permeability, indicating higher injection pressure and volume requirements. This can be attributed to larger pore throats contributing significantly to permeability. As a result, the influence of initial opening of microfractures on increasing pseudo-permeability is not prominently observed and necessitates more openings. This finding can be reverse validated by the fact that the impact of partial microfracture closure on the permeability of high-permeability cores was comparatively inferior to that observed in low-permeability cores under effective stress loading (Norbert and Georg, 2009). However, abnormal correlations were observed between pseudo-permeability at each injection pressure and initial permeability. For instance, compared to Q3, Q1 with the smallest initial permeability exhibited a similar pseudo-permeability at the injection pressure of 27 MPa.

The influence of fluid injection on permeability in tight sandstone primarily stems from rock deformation rather than colloid migration (Kozhevnikov et al., 2024). Therefore, the specific pseudo-permeability relies on the combination of microfracture opening and predominant manifestation in micropores. The assessment of the evolution of pore structure revealed microfracture opening in all three cores, which necessitates heightened attention toward micropores. This finding is consistent with the conclusion proposed by Nishiyama and Yokoyama (2017) that matrix pores play a crucial role in limiting the flow capacity in the matrix-fracture model. The

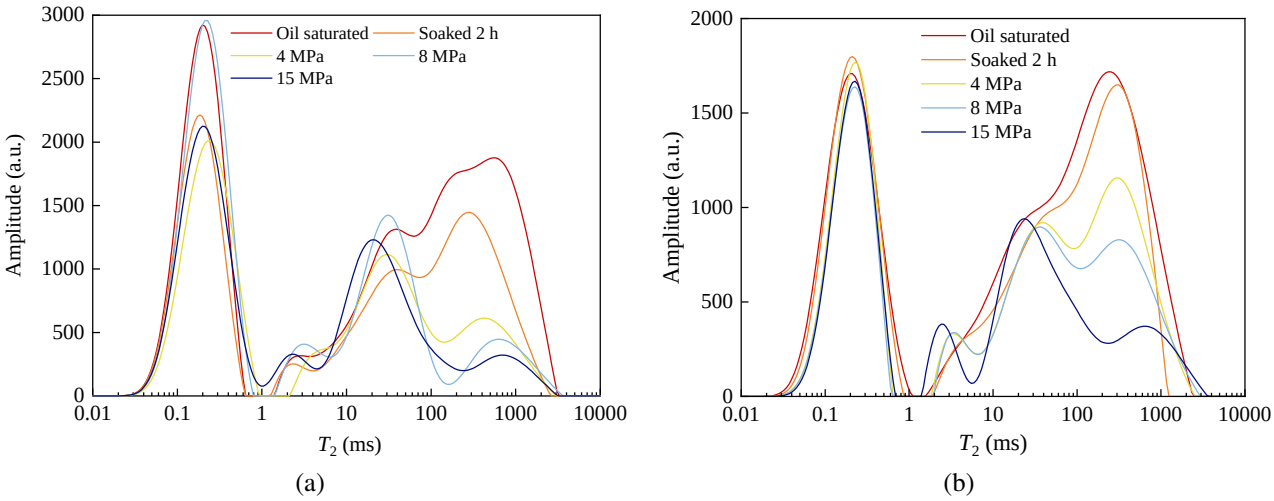


**Fig. 7**. NMR $T_2$ spectra of water huff and puff in different modes: (a) Massive injection in Q1 and (b) moderate injection in Q4.

minimal change observed in the micropores of Q1 suggests that pseudo-permeability is primarily influenced by microfracture opening, leading to higher values than others. Meanwhile, the unrecovered deformation on Q2 demonstrates irreversible rock damage and increases the flow resistance. Therefore, the flow capacity is inferior to that of Q1, and pseudo-permeability is diminished. The micropores in Q3 exhibit increased quantity, improved elastic recovery and enhanced flow capacity, hence its pseudo-permeability surpasses that of Q2. The flow capacity will be significantly enhanced until the flow balance between microfractures and matrix or the continuous opening of microfractures, which aligns with the right shift in its infection point. Therefore, when implementing massive energy replenishment at oilfields to maximize fluid flow capacity, careful attention must be paid to the combination of predominant micropore manifestation and microfracture opening.

## 3.2 Flow mechanism

### 3.2.1 Fluid movability

Fig. 7 depicts the NMR $T_2$ spectra of massive and moderate water huff and puff under different production pressure differences. The gradual decrease in spectral lines with increasing production pressure difference indicates oil movability in all pores under both energy replenishment modes. However, the two modes differ significantly in fluid movability. Furthermore, moderate water huff and puff exhibits an extended right endpoint ranging from 1,162.32 ms after soaking to 3,529.71 ms (Fig. 7(b)), indicating the oil enrichment in microfractures, which contrasts with massive water huff and puff.

The fluid movability under the two development modes (Fig. 8) can be calculated combining Fig. 7 and Eq. (3). The permeability differs in massive and moderate water huff and puff, measuring $0.064 \times 10^{-3}$ and $0.097 \times 10^{-3}$ μm$^2$, respectively (Table 1). However, it is noteworthy that the recovery degree at all production stages in Q1 surpasses that of Q4, indicating a significant enhancement in the recovery degree of cores with smaller permeability due to massive water huff and puff. This development mode enhances oil movability in all pores during soaking. In the production stage, there is a rapid increase in the recovery degree with a distinct inflection point at 4 MPa, followed by a more gradual increase as the production pressure differences increase (Fig. 8(a)). The recovery degree of macropores exhibits a continuous rise, while the oil saturation in micro-mesopores initially decreases and then increases. Conversely, the recovery degree and production pressure difference exhibit a linear relationship in moderate water huff and puff (Fig. 8(b)). This observation is related to the linear pressure distribution that is achieved once the fluid flow in the matrix reaches a steady state (Sun et al., 2023).

The above-listed data indicate that changes in the pressure sweep area and pore structure resulting from massive water huff and puff influence the recovery mechanism. Our findings on the evolution of physical properties demonstrate that massive injection significantly increases the pore pressure and the flow channels between water and matrix after microfracture opening. As a result, the injected water exhibits an improved ability to penetrate into matrix pores through microfractures with reduced flow resistance under the applied pressure. A significant improvement in mass transfer rate and capacity is observed between microfractures and matrix. Therefore, after a short soaking period, the recovery degree undergoes remarkable enhancement compared to moderate water huff and puff, accounting for 67.69% of the total recovery degree-twice that of the production stage (32.31%). Upon increasing the production pressure difference, the increase in flow channels and decrease in flow distance lead to an enhanced capacity and range for pressure sweep while reducing the oil drainage disconnection. Consequently, the recovery degree rapidly reaches its maximum value of 42.38% at a production pressure difference of 4 MPa, comparable to the achievement for Q4 at 15 MPa. Higher production pressure differences

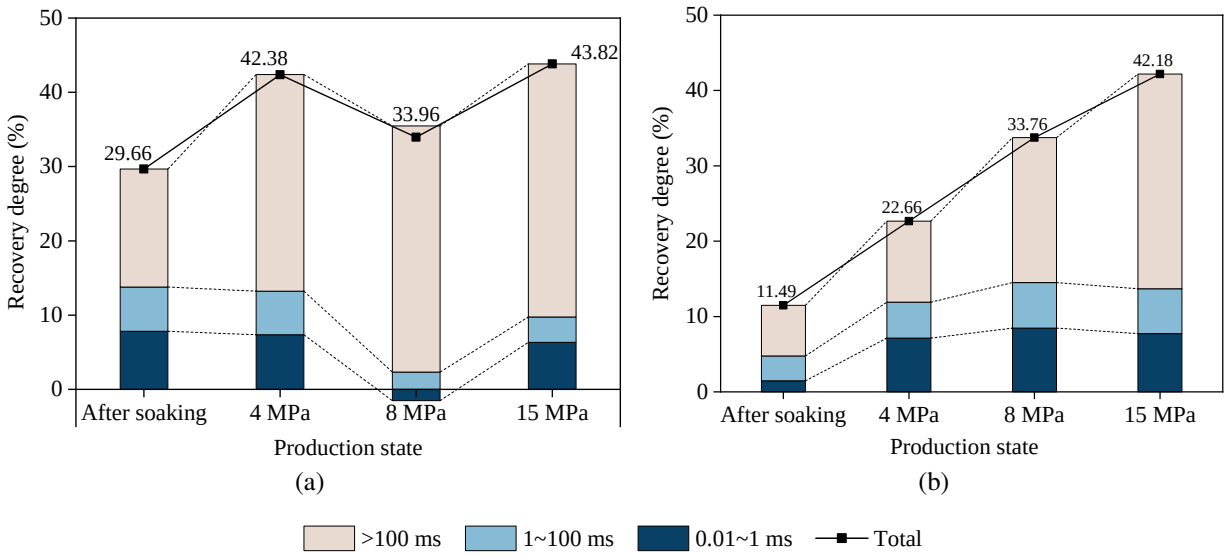


**Fig. 8**. Fluid movability of water huff and puff in different modes: (a) Massive injection in Q1 and (b) moderate injection in Q4.

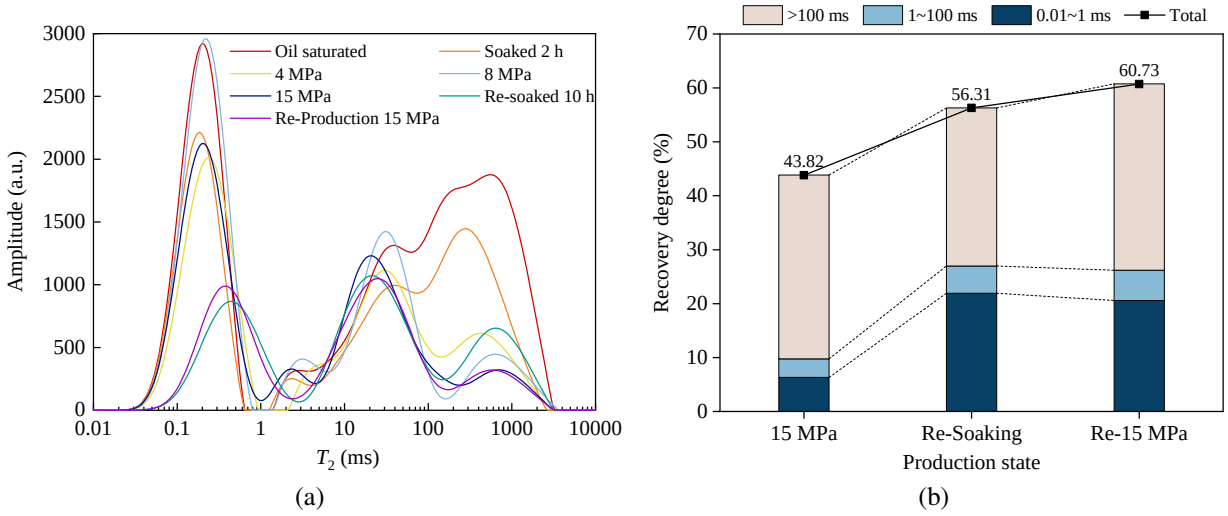


**Fig. 9**. Production characteristics of Q1 after re-soaking: (a) NMR $T_2$ spectra and (b) fluid movability.

can significantly enhance oil recovery in macropores and microfractures, with Q1 exhibiting a recovery degree of 5.58% higher than Q4. However, stable or increased oil saturation in micro-mesopores indicates oil backflow, leading to a low final recovery degree at 8 MPa during massive water huff and puff. To understand the underlying cause of this anomalous phenomenon, further analysis considering fluid migration is required. The recovery degree rebounds when the production pressure difference reaches 15 MPa; however, it still remains relatively low, making it the primary focus for subsequent development.

### *3.2.2 Effect of re-soaking on oil recovery*

In order to effectively mobilize fluid within micro-mesopores, Q1 was soaked for an additional 10 h according to the movability characteristics observed during soaking in massive water huff and puff. Fig. 9 presents the production characteristics after re-soaking. A significant decrease is observed in the left peak, while there is a slight drop in the middle accompanied by the disappearance of a small peak and an increase in the right peak (Fig. 9(a)). This observation suggests that re-soaking forces residual oil in mesopores to migrate into larger ones along with the oil drained from micropores and enriched in macropores. Thus, compared to initial production, there is a notable enhancement of 12.5% in the recovery degree (Fig. 9(b)). Furthermore, the right peak rapidly decreases during re-production at 15 MPa and nearly coincides with it before re-soaking. This phenomenon indicates that oil enriched in macropores is swiftly drained during re-production, resulting in an overall recovery degree approaching the upper limit.

The significant improvement in energy enhancement and

accumulation during soaking in massive water huff and puff leads to a notable enhancement in the recovery degree. However, in production, an effective combination of flooding and soaking is necessary to mobilize fluid within micro-mesopores, with the crucial parameters of injection volume and soaking timing.

### 3.2.3 Visualization of the flow mechanism

Based on the evolution of physical properties in massive energy replenishment and the fluid movability in massive water huff and puff, it is evident that the flow mechanism differs between massive and moderate water huff and puff (Figs. 10 and 11).

After massive water injection, closed microfractures gradually open with small openings due to the increased pore pressure. The narrow plane dramatically enhances imbibition efficiency and mass transfer during soaking, and the increased pore pressure assists the viscous driving force to overcome the capillary force within micropores for imbibition and drainage (white circle below, Fig. 10(b)). Simultaneously, the pronounced reduction in flow distance and resistance facilitates the migration and enrichment of drained oil into macropores at the outlet, driven by improved energy enhancement and accumulation resulting from high-pressure injection (white circle above, Fig. 10(b)).

The increase in pore pressure and production pressure difference after soaking facilitates the rapid drainage of oil enriched in macropores and microfractures, driven by viscous forces (Figs. 10(c) and 10(d)). Simultaneously, the viscous resistance exerted by single-phase oil on pore walls and the flow resistance of oil-water two-phase are offset for the above two reasons, thereby significantly enhancing the oil washing efficiency within macropores (Figs. 10(e) and 10(f)). However, the injected water can readily establish a preferential flow path at a specific pore throat level due to its tendency toward minimum energy. Once the oil droplets precipitated or the oil film adsorbed on the microfracture walls of this path are almost entirely stripped away, the two-phase flow transitions into a single-phase flow dominated by the injected water. As the injection front at the inlet and the pressure continue to sweep towards the deep matrix, the injected water volume imbibing into the matrix decreases while water saturation continues to increase. Consequently, the migration of drained oil droplets in the matrix pores primarily relies on the carry-over and extrusion effect of injected water, potentially leading to their backflow to micro-mesopores or even the deeper matrix. This process leads to fluctuations in oil saturation within these pores until imbibition occurs again as a result of oil accumulation in the micropores (white circle, Fig. 10(e)). These findings are similar to the proposition by Li et al. (2022b) regarding the carry-over and flushing effects in multiple cycles of water injection. At present, continuous increases in production pressure differences are ineffective in oil recovery, leading to a dynamic balance between water injection and oil production. Re-soaking results in increased oil drainage through imbibition from micropores towards the outlet for enrichment, which is attributed to the prolonged massive injection and the enhanced energy enhancement and accumulation (white circle, Fig. 10(k)). Ultimately, oil is recovered during re-production.

During moderate water huff and puff, the limited penetration of injected water into matrix pores in soaking poses a challenge in changing the oil distribution (Figs. 11(a) and 11(b)). The primary flow mechanism relies on increased production pressure difference and prolonged production time for the injected water to gradually sweep towards the deep matrix. Due to a longer contact time between injected water and matrix pores at the inlet, oil drainage from these pores is extended (Figs.11(c) and 11(d)). Thus, the increase in production pressure difference leads to the drained oil droplets progressively migrating towards macropores at the outlet over a long flow distance and duration, indicated by a shift in oil saturation towards larger $T_2$ at the outlet (white arrows, Figs. 11(e) and 11(f)).

As a consequence, massive water huff and puff in the oilfield can significantly enhance the energy field and fluid flow capacity for a substantial enhancement of oil recovery.

## 4. Conclusions

The present study designed an online NMR simulation experimental method integrating “injection, soaking and production” for massive energy replenishment and simulated its dynamic flow process. On the one hand, the findings elucidated the evolution of rock physical properties and massive energy replenishment mechanism. On the other hand, the fluid movability and flow mechanism in massive water huff and puff were revealed. This work provides a theoretical basis for understanding massive energy replenishment. The following main conclusions could be drawn:

1) The evolution of pore structure primarily involves microfractures and micropores, which can be classified into two stages based on injection volume: Initial opening of microfractures and deformation of partial larger pores during the injection of small volumes, followed by the rapid opening of microfractures and the partial elastic recovery of deformation under massive fluid injection.
2) Massive energy replenishment can promote the involvement of more pore throats in the flow. However, the flow capacity increase varies across different locations, with a more pronounced increase observed at the inlet than others. A larger fluid injection volume leads to an enhanced opening degree of microfractures. The increase in permeability positively influences fluid movability within micro-mesopores.
3) The increase in pseudo-permeability exhibits an exponential increase with the injection volume during massive energy replenishment, and its inflection point presents a positive correlation with initial permeability. The pseudo-permeability for each injection volume primarily relies on the combined influence of microfracture opening and dominant manifestation of micropores.
4) Massive water huff and puff can significantly enhance oil recovery by increasing pore pressure and the number of flow channels. It achieves a remarkable energy enhancement and accumulation effect after soaking, leading

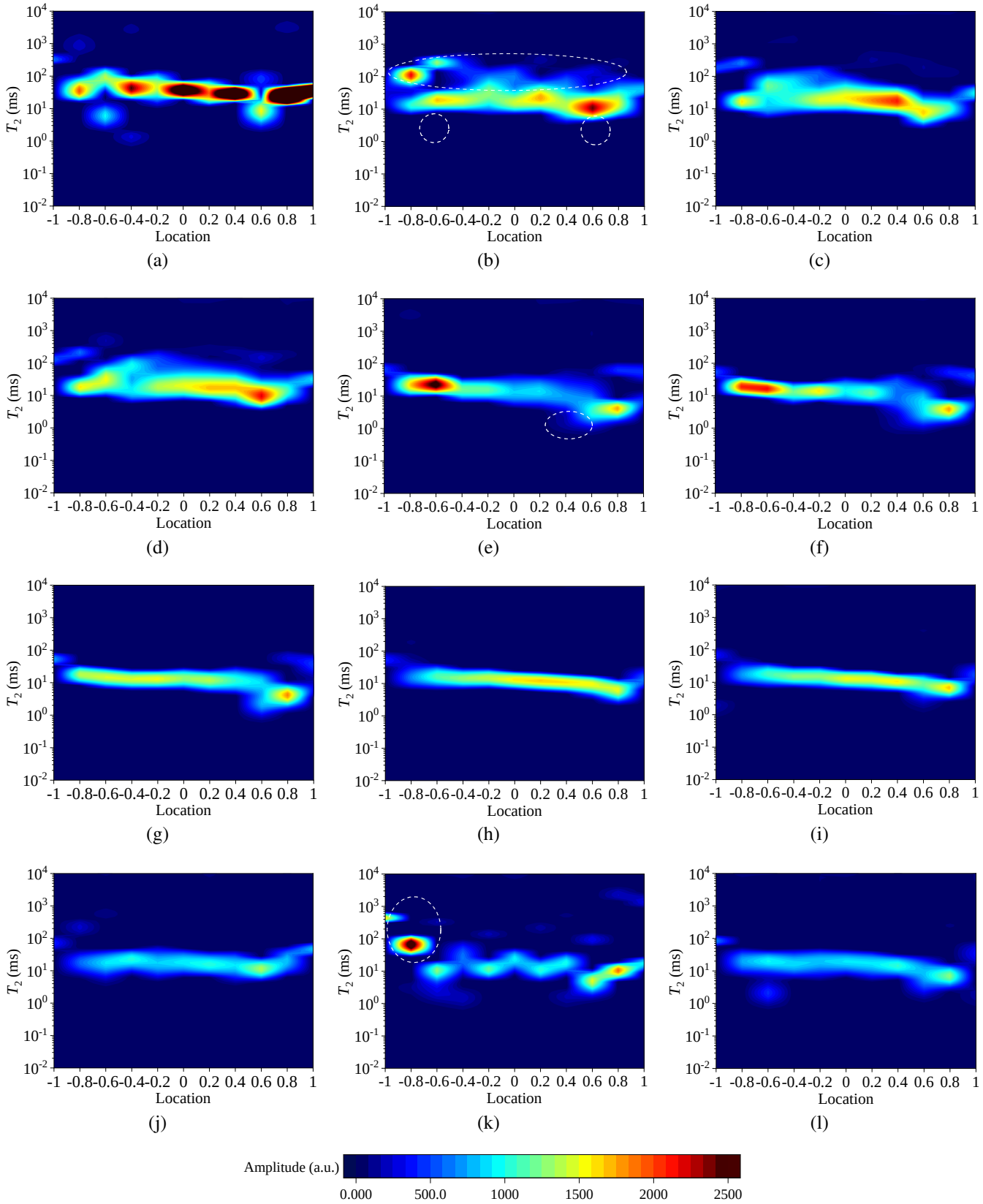


**Fig. 10**. Fluid migration in massive water huff and puff in Q1: (a) Oil saturated state, (b) after soaking, (c) 4 MPa (1 h), (d) 4 MPa (2 h), (e) 8 MPa (1 h), (f) 8 MPa (2 h), (g) 8 MPa (3 h), (h) 8 MPa (5 h), (i) 15 MPa (1 h), (j) 15 MPa (3 h), (k) re-soaking and (l) re-production at 15 MPa.

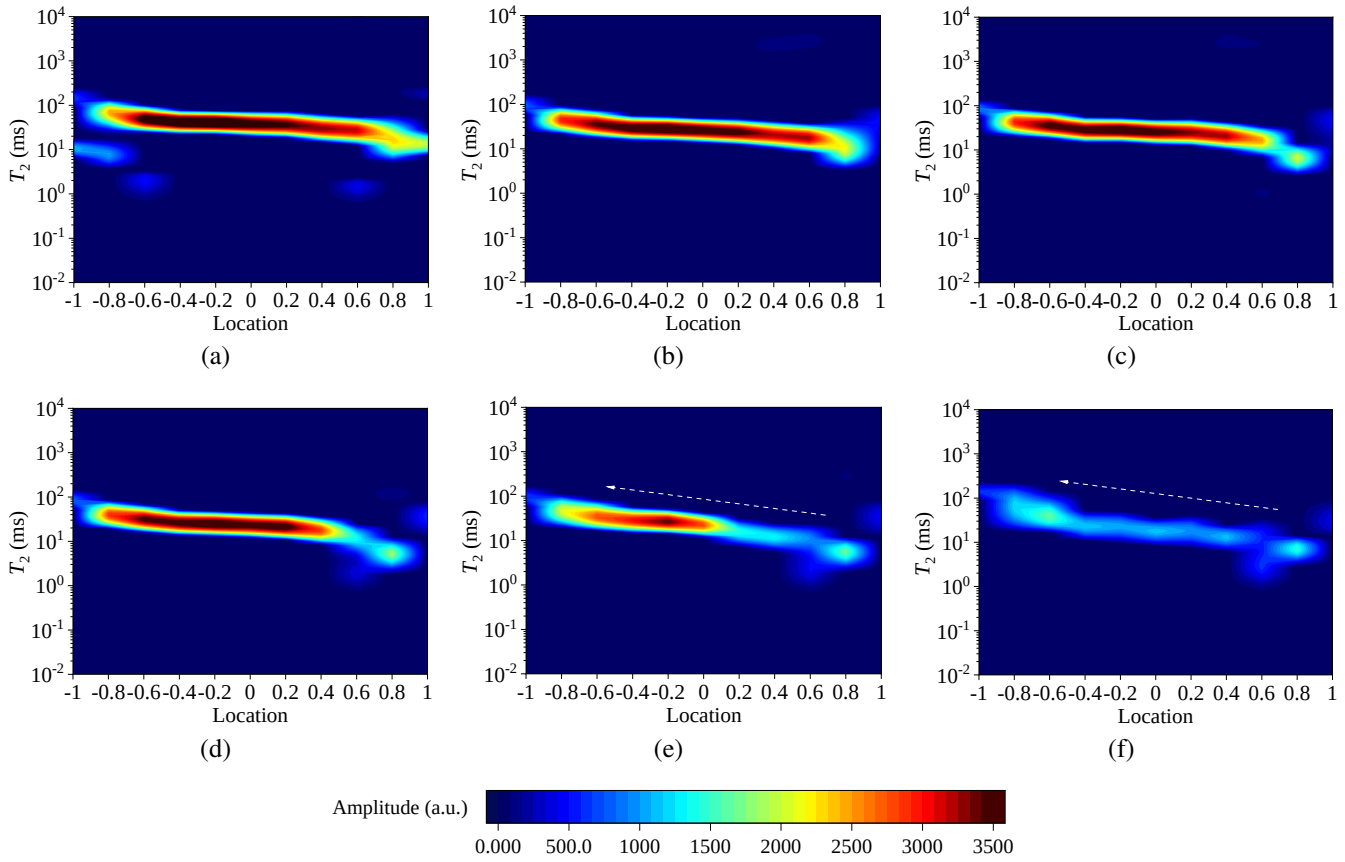


**Fig. 11**. Fluid migration in moderate water huff and puff in Q4: (a) Oil saturated state, (b) after soaking, (c) 4 MPa (1 h), (d) 4 MPa (1.5 h), (e) 8 MPa and (f) 15 MPa.

to a substantial migration and enrichment of oil drained by imbibition towards macropores at the outlet. The inflection point of the recovery degree enhancement is observed under a small production pressure difference and production time. However, the increasing production pressure difference does not effectively mobilize the fluid in micro-mesopores due to the carry-over and extrusion effect of water phase on oil droplets in the matrix. Therefore, it is imperative to integrate flooding and soaking, with careful consideration of the injection volume and the soaking timing.

## Acknowledgements

This work was financially supported by the National Key Research and Development Program of China (No. 2023YFF0614100), and the Scientific Research and Technology Development Project of China National Petroleum Corporation (Nos. 2023ZZ04-01 and 2021ZZ01-03).

The authors are grateful to Dr. Xinliang Chen and Dr. Meng Du for their precious suggestions.

## Conflict of interest

The authors declare no competing interest.



## References

Abou-Sayed, A. S., Zaki, K. S., Wang, G., et al. A mechanistic model for formation damage and fracture propagation during water injection. Paper SPE 94606 Presented at SPE European Formation Damage Conference and Exhibition, Sheveningen, The Netherlands, 25-27 May, 2005.

Anderson, W. G. Wettability literature survey part 5: The effects of wettability on relative permeability. Journal of Petroleum Technology, 1987, 39(11): 1453-1468.

Bodini, S. A., Forni, L. P., Tuero, F., et al. Unconventional EOR: Field tests results in Vaca Muerta Shale Play: A capillary based improved oil recovery case study for shale/tight oil scenarios. Paper SPE 191877 Presented at the SPE Argentina Exploration and Production of Unconventional Resources Symposium, Neuquen, Argentina, 14-16 August, 2018.

Cheng, L., Wang, D., Cao, R., et al. The influence of hydraulic fractures on oil recovery by water flooding processes in tight oil reservoirs: An experimental and numerical approach. Journal of Petroleum Science and Engineering, 2020, 185: 106572.

Chevalier, T., Chevalier, C., Clain, X., et al. Darcy's law for yield stress fluid flowing through a porous medium.

Journal of Non-Newtonian Fluid Mechanics, 2013, 195: 57-66.

David, C., Wong, T., Zhu, W., et al. Laboratory measurement of compaction-induced permeability change in porous rocks: Implications for the generation and maintenance of pore pressure excess in the crust. Pure and Applied Geophysics, 1994, 143: 425-456.

Gadde, P. B., Sharma, M. M. Growing injection well fractures and their impact on waterflood performance. Paper SPE 115204 Presented at SPE Annual Technical Conference and Exhibition, New Orleans, Louisiana, 23-25 September, 2001.

Golsanami, N., Sun, J., Zhang, Z. A review on the applications of the nuclear magnetic resonance (NMR) technology for investigating fractures. Journal of Applied Geophysics, 2016, 133: 30-38.

Haghi, A. H., Chalaturnyk, R., Geiger, S. New semi-analytical insights into stress-dependent spontaneous imbibition and oil recovery in naturally fractured carbonate reservoirs. Water Resources Research, 2018, 54: 9605-9622.

Hagoort, J. Waterflood-induced hydraulic fracturing. Delft, Delft Technical University, 1981.

Ji, W., Yu, H., Liu, X., et al. Oil production mechanism of water injection huff-n-puff for enhancing oil recovery in tight sandstone reservoir. Energy & Fuels, 2023, 37(23): 18867-18877.

Kozhevnikov, E., Turbakov, M., Riabokon, E., et al. Rock permeability evolution during cyclic loading and colloid migration after saturation and drying. Advances in Geo-Energy Research, 2024, 11(3): 208-219.

Li, S., Yang, S., Dong, W., et al. Influence of water injection pressure and method on oil recovery of water injection huff and puff in tight volcanic oil reservoirs. ACS Omega, 2022a, 7(25): 21595-21607.

Li, S., Yang, S., Gao, X., et al. Experimental study on liquid production law, oil recovery mechanism, and influencing factors of water huff-n-puff in the tight sedimentary tuff oil reservoir. Journal of Petroleum Science and Engineering, 2022b, 208(Part D): 109721.

Li, S., Yang, S., Jin, L., et al. Study on influencing factors of water huff-n-puff oil recovery in matrix-fracture systems of the tight sedimentary tuff reservoirs. ACS Omega, 2022c, 7(36): 32250-32261.

Ma, N., Li, C., Wang, F., et al. Laboratory study on the oil displacement process in low-permeability cores with different injection fluids. ACS Omega, 2022, 9(7): 8013-8022.

Milad, M., Junin, R., Sidek, A., et al. Huff-n-puff technology for enhanced oil recovery in shale/tight oil reservoirs: Progress, gaps, and perspectives. Energy & Fuels, 2021, 35(21): 17279-17333.

Nishiyama, N., Yokoyama, T. Permeability of porous media: Role of the critical pore size. Journal of Geophysics Research: Solid Earth, 2017, 122: 6955-6971.

Norbert, Z., Georg, N. Anisotropy of permeability and complex resistivity of tight sandstones subjected to hydrostatic pressure. Journal of Applied Geophysics, 2009, 68(3): 356-370.

Norris, J. Q., Turcotte, D. L., Rundle, J. B. A damage model for fracking. International Journal of Damage Mechanics, 2015, 24(8): 1227-1238.

Pearse, J., Singhroy, V., Samsonov, S., et al. Anomalous surface heave induced by enhanced oil recovery in northern Alberta: Insar observations and numerical modeling. Journal of Geophysical Research: Solid Earth, 2014, 119(8): 6630-6649.

Qin, G., Dai, X., Sui, L., et al. Study of massive water huff-n-puff technique in tight oil field and its field application. Journal of Petroleum Science and Engineering, 2021, 196: 107514.

Radwan, A. E., Wood, D. A., Abudeif, A. M., et al. Reservoir formation damage; reasons and mitigation: A case study of the Cambrian-Ordovician Nubian 'C' sandstone gas and oil reservoir from the gulf of Suez Rift Basin. Arabian Journal for Science and Engineering, 2022, 47: 11279-11296.

Sanchez-Rivera, D., Mohanty, K., Balhoff, M. Reservoir simulation and optimization of huff-and-puff operations in the Bakken Shale. Fuel, 2015, 147: 82-94.

Sun, L., Li, M., Abdelaziz, A., et al. An efficient 3D cell-based discrete fracture-matrix flow model for digitally captured fracture networks. International Journal of Coal Science & Technology, 2023, 10: 70.

Sun, Y., Chen, C., Ma, S., et al. Hydrocarbon accumulation characteristics and its main controlling factors in lithologic reservoirs area: Example of Fuyu oil layer in the southern Fuxin uplift of Songliao Basin. Advanced Materials Research, 2012, 524: 134-139.

Sun, Y., Deng, M., Ma, S., et al. Distribution and controlling factors of tight sandstone oil in Fuyu oil layers of Da'an area, Songliao Basin, NE China. Petroleum Exploration and Development, 2015, 42(5): 646-655.

Thomas, R. D., Don, C. W. Effect of overburden pressure and water saturation on gas permeability of tight sandstone cores. Journal of Petroleum Technology, 1972, 24: 120-124.

Todd, H. B., Evans, J. G. Improved oil recovery IOR pilot projects in the Bakken formation. Paper SPE 180270 Presented at the SPE Low Perm Symposium, Denver, USA, 5-6 May, 2016.

Umeobi, H. I., Li, Q., Xu, L., et al. NMR Investigation of brine imbibition dynamics in pores of tight sandstones under different boundary conditions. Energy & Fuels, 2021, 35(19): 15856-15866.

Vairogs, J., Vaughan, W. R. Pressure transient tests in formations having stress-sensitive permeability. Journal of Petroleum Technology, 1973, 25(8): 965-970.

Van Den Hoek, P. J. Pressure transient analysis in fractured produced water injection wells. Paper SPE 77946 Presented at SPE Asia Pacific Oil and Gas Conference and Exhibition, Melbourne, Australia, 8-10 October, 2002.

Van Den Hoek, P. J., Hustedt, B., Sobera, M., et al. Dynamic induced fractures in waterfloods and EOR. Paper SPE 115204 Presented at SPE Russian Petroleum Technology Conference, Moscow, Russia, 28-30 October, 2008.

Wang, W., Peng, Y., Li, G., et al. Opening mechanism of

dynamic fractures caused by water injection and effective adjustments in low permeability reservoirs, Daqing oilfield in Songliao Basin. Oil & Gas Geology, 2015a, 36(5): 842-847. (in Chinese)

Wang, Y., Cheng, S., Zhang, K., et al. Case studies: Pressure-transient analysis for water injector with the influence of waterflood-induced fractures in tight reservoir. Paper SPE 190264 Presented at the SPE Improved Oil Recovery Conference, Tulsa, USA, 14-18 April, 2018a.

Wang, Y., Cheng, S., Zhang, K., et al. Impact of shrinking fracture length and decreasing fracture conductivity on bottom-hole pressure performance: A semi-analytical model to characterize waterflood-induced fracture around water injection well. Paper SPE 190060 Presented at the SPE Western Regional Meeting Held in Garden Grove, California, USA, 22-27 April, 2018b.

Wang, Y., Song, X., Tian, C., et al. Dynamic fractures are an emerging new development geological attribute in waterflooding development of ultra-low permeability reservoirs. Petroleum Exploration and Development, 2015b, 42(2): 247-253.

Wijaya, N., Sheng, J. J. Shut-in effect in removing water blockage in shale-oil reservoirs with stress-dependent permeability considered. SPE Reservoir Evaluation & Engineering, 2020, 23(1): 81-94.

Wu, Z., Zeng, Q., Li, J. New effective energy-supplement development method of waterflood huff and puff for the oil reservoir with stimulated reservoir volume fracturing. Petroleum Geology and Recovery Efficiency, 2017, 24(5): 78-83+92. (in Chinese)

Zhao, J., Fan, J., He, Y., et al. Optimization of horizontal well injection-production parameters for ultra-low permeable-tight oil production: A case from Changqing Oilfield, Ordos Basin, NW China. Petroleum Exploration and Development, 2015, 42(1): 74-82.

Zhong, X., Zhu, Y., Liu, L., et al. The characteristics and influencing factors of permeability stress sensitivity of tight sandstone reservoirs. Journal of Petroleum Science and Engineering, 2020, 191: 107221.

Zhou, X., Wang, Y., Zhang, L., et al. Evaluation of enhanced oil recovery potential using gas/water flooding in a tight oil reservoir. Fuel, 2020, 272: 117706.